Determination of Multivalent Protein-Ligand Binding Kinetics Using Second Harmonic Correlation Spectroscopy

*Krystal L. Sly and John C. Conboy**

Department of Chemistry, University of Utah, 315 South 1400 East RM. 2020, Salt Lake City, Utah 84112

*conboy@chem.utah.edu

SUPPORTING INFORMATION

1. Materials. 1,2-dioleoyl-*sn*-glycero-3-phosphocholine (DOPC), 1,2-dioleoyl-sn-glycero-3-phosphoethanolamine-N-(lissamine rhodamine B sulfonyl) (Rh-DOPE), and monosialotetrahexosyl ganglioside (GM_1) (Ovine Brain) were purchased from Avanti Polar Lipids and used as received. Immunoglobulin G from Rabbit serum (IgG), cholera toxin B subunit from *Vibrio cholera* (CTB), and *arachis hypogaea* from peanut agglutinin (PnA) were obtained from Sigma-Aldrich. The water used in these experiments was purified using a Nanopure^{TM} Infinity Ultrapure water system with a minimum resistivity of 18.2 MΩ-cm. The 150 mM solution of phosphate buffered saline (PBS) composed of 50 mM $Na_2HPO_4 \cdot 7H_20$ and 100 mM NaCl in water was adjusted to the physiological pH of 7.4 using NaOH. Both CTb and

PnA were dissolved in PBS pH 7.4 to the desired working concentrations (0.22 nM to 240 nM for CTB and 0.43 μM to 12.02 μM for PnA).

2. Formation of PSLBs. Planar supported lipid bilayers (PSLBs) were formed on custom manufactured full spectrum grade (IR/UV) fused silica prisms (Almaz Optics). The prisms were first cleaned by submersion in a solution a 70 to 30 sulfuric acid to hydrogen peroxide solution overnight (CAUTION: *this solution is a strong oxidant and reacts violently with organic solvents. Extreme caution must be taken when handling the solution*). The prisms were then rinsed with an ample amount of water and then Ar plasma cleaned (Harrick Scientific Plasma Cleaner/Sterilizer) for 2-3 minutes. The DOPC lipids used in these experiments were dissolved in chloroform and doped with GM_1, which had been dissolved in a 1:1 chloroform:methanol mixture. The GM_1 density was chosen such that there would be a monolayer of protein at the surface when the binding sites had been saturated (1 mol % for CTB and 5 mol % for PnA). All lipids were dried under a gentle stream of N_2 (g) followed by vacuum drying for at least 4 hours to remove residual solvent. The dried lipids were stored in a − 20°C freezer until they were used. Small unilamellar vesicle (SUV) solutions were prepared by re-suspending the dried lipids in PBS to a concentration of 1 mg/mL followed by vortexing and bath sonication for 10-20 minutes until the solutions were clear. A PSLB was formed on the silica prism by vesicle fusion by incubating the surface with the SUV solution for 20 minutes at room temperature upon which the SUVs spontaneously rupture to form a uniform lipid bilayer. Excess PBS was flushed through the flowcell to remove any unbound lipids in solution. To screen any possible defects on the bilayer and prevent non-specific binding of the proteins, the PSLBs were incubated with IgG for 30 minutes and then rinsed with PBS to remove any unbound IgG in solution. The uniformity of the bilayers prepared by this method was examined by fluorescence microscopy (shown in

Figure S1). A DOPC PSLB containing 1 mol % Rh-DOPE and 5 mol% GM_1 was formed via vesicle fusion on the surface of a quartz coverslip and a fluorescence image was obtained of the resulting PSLB (Figure S1A) using an Olympus BX40 fluorescence microscope equipped with a Photmetrics CoolSNAP$_{cf}$ (Roper Scientific) color camera and a 557/571 excitation/emission filter set. The image was obtained using a 50x objective (NA, 0.50) with an exposure time of 0.1 seconds. A fluorescence image was also obtained after IgG and 240 nM CTB was incubated with the GM_1 doped DOPC bilayer (shown in Figure S1B). The PSLB was uniform before and after binding of the protein.

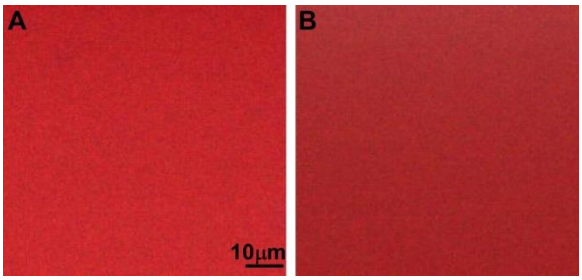

Figure S1. Fluorescence microscopy image of a 5 mol% GM_1 doped DOPC bilayer with 1 mol% Rh-DOPE A) before incubation with protein and B) after incubation with IgG and 240 nM CTB.

3. SHG Measurements. Counter-propagating SHG was used for these experiments and is described in detail elsewhere.[1] The second harmonic output (532 nm) of a Nd:YAG laser (Continuum, Surelite II, 20 Hz, 7ns pulse) was sent towards a prism/water interface under total internal reflection. The measured laser power at the sample was 20-24 mJ/pulse and the beam size was ~ 1 mm^2 in diameter. A mirror guided the reflected beam back on itself such that it overlapped spatially and temporally with the incident beam, producing an SH emission at 266 nm along the surface normal. Two notch filters (Semrock co.) with 64% transmittance at 266 nm placed in the path of the emitted beam permitted only the SH signal to be collected by the solar-blind photomultiplier tube (Hamamatsu). It is important to note that extreme care must be taken to align the cavity of the laser and optimize the beam intensity distribution, as these parameters

greatly affect the noise of the correlation data. In order to reduce the noise introduced from the laser, the xenon flashlamps were only used to about half their usual lifetime, as the noise of the laser significantly increases as the flashlamps age. Maintaining the laser so it is stable assures that most of the noise seen in the correlation data is due to the detection system shot noise and not noise from the laser and associated optics.

The measured SH signal is proportional to the second-order susceptibility tensor, $\chi_{ijk}^{(2)}$ which is composed of both a non-resonant $\chi_{NR}^{(2)}$ and resonant $\chi_{R}^{(2)}$ portion:

$$I_{SHG} \propto \left|\chi_{ijk}^{(2)}\right|^2 \propto \left|\chi_{NR}^{(2)} + \chi_{R}^{(2)}\right|^2. \quad \text{(S1)}$$

The resonant $\chi_{R}^{(2)}$ contribution can be expressed as:[2]

$$(\chi_{ijk}^{(2)})_R \propto N \sum_{a,b,c} \frac{\langle a|\mu_i|c\rangle\langle a|\mu_j|b\rangle\langle b|\mu_k|c\rangle}{(2h\omega - E_{ca} - i\Gamma_{ca})(h\omega - E_{bc} - i\Gamma_{bc})} \quad \text{(S2)}$$

where *N* is the surface density of molecules, *h* is Planck's constant, μ is the Cartesian coordinate dipole operator, Γ is the transition linewidth of the laser, and *a*, *b* and *c* represent the initial, intermediate, and final states, respectively. The indices on $\chi_{ijk}^{(2)}$ denote the input (*j*,*k*) and output (*i*) fields, which can assume any of the three Cartesian coordinates (*x*,*y*,*z*). The SH signal is enhanced when the incident (ω) or SH (2ω) frequency is resonant with an electronic transition of a molecule at the surface, as shown in the denominator of Equation S2. With this resonant enhancement, very low concentrations of molecules at the surface can be detected using SH spectroscopy. This means that if the analyte being detected has an electronic transition at the frequency of the SH light there will be a lower limit of detection (LOD) and increased sensitivity.[3]

Here, a fundamental wavelength of 532 nm is used such that the resulting SH wavelength is 266 nm, which is in resonance with the electronic transition of the tryptophan and tyrosine

residues in the proteins used in this study (shown in Figure S2). The signal enhancement from this resonance allows detection down to low nM concentrations of CTB and μM concentrations of PnA, giving LODs of 0.7 ± 0.01 femtomoles/cm^2 and 40.3 ± 3.7 femtomoles/cm^2, respectively. These LODs are similar to those reported using fluorescence and lower than those reported using QCM to monitor the binding of these proteins to immobilized ligand surfaces.[4,5]

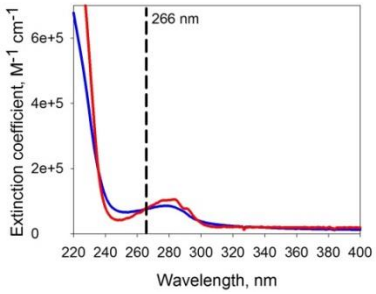

Figure S2. Extinction coefficient spectra of CTB (blue) and PnA (red).

4. Adsorption Isotherms. SH binding isotherms of the proteins associating to GM_1 doped in DOPC bilayers were performed in duplicate for CTB and triplicate for PnA. Any changes in the laser power between experiments was compensated for by performing a two-point normalization to a 10 mM KOH solution and a solution of PBS pH 7.4, followed by subtraction of the background SH intensity before any protein was added. The SH intensity was monitored over time as increasing concentrations of the proteins were injected and allowed to reach equilibrium between the bulk solution and bilayer. The depletion of the bulk protein concentration as proteins bound to the surface was offset by injecting a fresh solution of the same protein concentration every 10 minutes until a steady-state response was reached. For the lowest concentration of CTB it required up to 14 hours to reach steady-state equilibrium. Since the lowest concentration of PnA was in the μM range the time required to reach equilibrium was shortened to 2 hours. Each data point collected was averaged for 100 samples and integrated using a boxcar. To prevent

damage to the bilayer from exposure to the laser, the SH intensity was recorded at 5-10 min intervals for 2-3 minutes and then blocked. The thermodynamic equilibrium binding constant was determined from an isotherm consisting of only the SH intensity collected at steady-state equilibrium for each protein concentration.

5. CTB Single-Shot Raw Data. Figure S3 are representative examples of the measured fluctuations in SH signal that were used to obtain the autocorrelation function found in Figure 1.

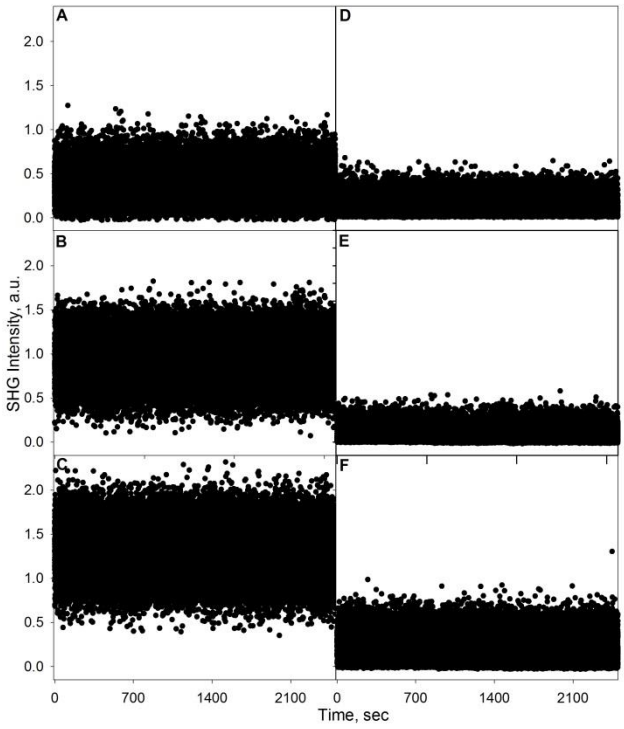

Figure S3. Single shot raw data for CTB binding to a 1 mol % GM1 doped DOPC bilayer at CTB concentrations 0.5 nM (A), 13 nM (B), and 240 nM (C) and CTB binding to a pure DOPC bilayer at CTB concentrations 0.5 nM (D), 13 nM (E), and 240 nM (F).

6. Electrostatics of CTB. The electrostatic map for the binding plane (Figure S4A) and top plane (Figure S4B) of CTB was (PDB: 1PZJ) calculated in Python Molecular Viewer from Scripps MGL tools assuming a 150 mM salt concentration.[6]

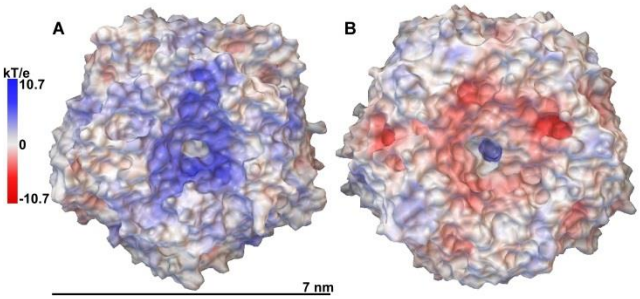

Figure S4. Electrostatic potential map for the binding plane (A) and top plane (B) of CTB (PDB: 1PZJ) where red indicates negative potential, white is neutral and blue is indicative of positive potential.

7. CTB Desorption

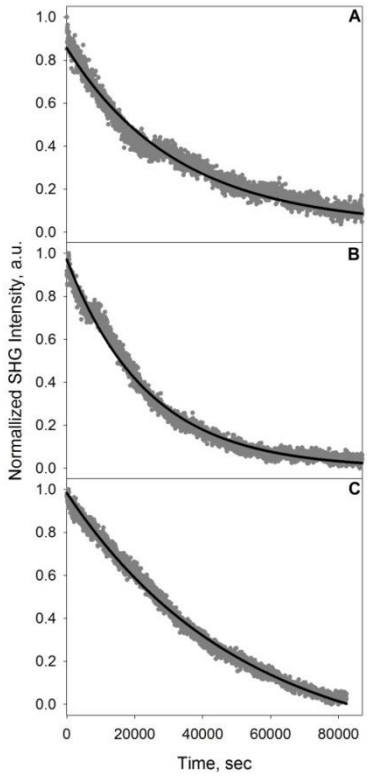

Figure S6. SH intensity vs. time for the desorption of CTB bulk concentration (A) 0.5 nM, (B) 13 nM, and (C) 240 nM. Solid lines are the fits to an exponential decay for the three CTB concentrations.

8. Hill-Waud Equation. In equation S1 it is shown that the SH intensity is proportional to second order susceptibility tensor which is composed of both a resonant and nonresonant portion.

The non-resonant $\chi_{NR}^{(2)}$ is real, as there are no electronic resonances from the lipids, water or silica in the spectral region of interest. However, since the SH frequency is on resonance with electronic transitions of the protein (Figure S1) the resonant $\chi_{R}^{(2)}$ is a complex number. The SH intensity can be rewritten as:

$$I_{SHG} \propto \left|\chi^{(2)}\right|^2 \propto |A + N(B + iC)|^2 \propto (A + NB)^2 + (NC)^2 \,, \tag{S3}$$

where *A* represents the non-resonant response from the background before addition of protein, and *B* and *C* denote the real and imaginary components of the resonant susceptibility from the protein, respectively.

If there are multiple identical binding sites and ligand-ligand interactions, the surface adsorption of the protein is described by the Hill-Waud model where the surface density *N* in equation S3 is given by:

$$N = \frac{N_{max} K_a^n [P]^n}{1 + K_a^n [P]^n}, \tag{S4}$$

where N_{max} is the maximum surface density at saturation, K_a is the equilibrium binding constant, *[P]* is the bulk protein concentration, and *n* is the Hill coefficient, which describes the affinity of the protein for its ligand when another ligand is already bound. Using the relationship between the surface density and the SH intensity, $I_{SHG} \propto N^2$, and subtracting the background SH intensity, $I_{SHG}^{background}$, designated as *A*, the SH intensity from the adsorption of protein in terms of the Hill-Waud model can be expressed by the following:

$$I_{SHG} - I_{SHG}^{background} \propto 2B\sqrt{I_{SHG}^{background}}\left(\frac{\sqrt{I_{SHG}^{max}} K_a^n [P]^n}{1 + K_a^n [P]^n}\right) + (B^2 + C^2)\left(\frac{\sqrt{I_{SHG}^{max}} K_a^n [P]^n}{1 + K_a^n [P]^n}\right)^2. \tag{S5}$$

Since the SH signal is on resonance with an electronic transition of CTB (Figure 1), *B* is much smaller than the imaginary portion of the resonant susceptibility tensor, making ($B^2 + C^2$) much

greater than the cross-term $2B\sqrt{I_{SHG}^{background}}$.[7] Additionally, ($B^2$ + C^2) relates to the surface density of molecules and can therefore be combined into $\sqrt{I_{SHG}^{max}}$. Using these simplifications, the Hill-Waud model in terms of the SH intensity takes the form of equation 8.

9. PnA Single-Shot Raw Data. Figure S7 are representative examples of the measured fluctuations in SH signal that were used to obtain the autocorrelation function found in Figure 3.

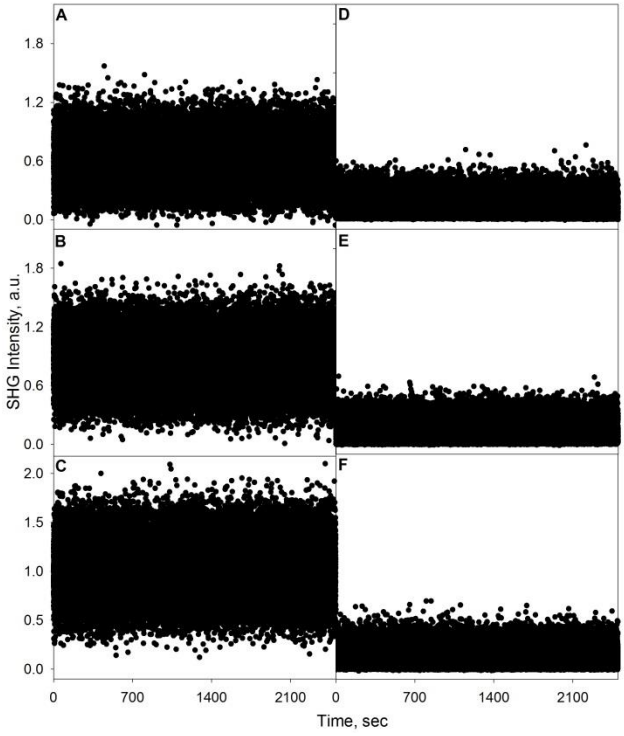

Figure S7. Single shot raw data for PnA binding to a 5 mol % GM1 doped DOPC bilayer at PnA concentrations 0.43 μM (A), 3 μM (B), and 12 μM (C) and PnA binding to a pure DOPC bilayer at PnA concentrations 0.43 μM (D), 3 μM (E), and 12 μM (F).

10. Electrostatics of PnA. The electrostatic map of PnA (PDB: 2PEL) was calculated in Python Molecular Viewer from Scripps MGL tools assuming a 150 mM salt concentration.[6]

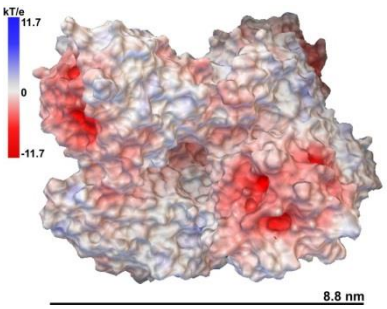

Figure S8. Electrostatic potential map of PnA (PDB: 2PEL) where red indicates negative potential.

11. Adsorption and Desorption of PnA. To further probe the effects of mass transport on the predicted K_a, separate adsorption and desorption experiments were performed for PnA concentrations of 0.43 μM, 3 μM and 12 μM. The SH intensity was monitored over time as each bulk PnA concentration was adsorbed to 5 mol % GM_1 doped into a DOPC bilayer. After a fresh protein solution was injected to replenish the bulk protein concentration, the SHG intensity was collected every 5-10 minutes for 2-3 minutes until steady-state equilibrium had been reached (data shown in Figure S9A). Once steady-state equilibrium had been reached, the PnA was desorbed by flushing a copious amount of buffer over the surface and collecting the SH signal every 15 seconds (data shown in Figure S9B). The adsorption data (Figure S9A) were fit to the an exponential rise model with the form of,

$$I_{SHG} = a(1 - exp^{-bx}), \tag{S6}$$

where a is the amplitude at the maximum and b is equal to $k_{on}[P] + k_{off}$. The desorption data (Figure S8B) were fit to an exponential decay to obtain k_{off}. The desorption rates for PnA concentrations of 0.43 μM, 3 μM and 12 μM were 2.2 ± 0.7 × 10^{-3} s^{-1}, 2.4 ± 0.1 × 10^{-3} s^{-1}, and 4.1 ± 1.2 × 10^{-3} s^{-1}, respectively. Using these desorption rates, the adsorption rates for PnA concentrations of 0.43 μM, 3 μM and 12 μM were calculated as 1.4 ± 0.5 × 10^3 $M^{-1}s^{-1}$, 5.8 ± 0.4 × 10^2 $M^{-1}s^{-1}$, and 1.5 ± 0.4 × 10^2 $M^{-1}s^{-1}$, respectively. Although the adsorption rates are not

identical to those measured using SHCS, all three of the desorption rates are in good agreement with those measured by SHCS. Interestingly, the same inverse relationship between the binding kinetics and PnA concentration is apparent in both the adsorption data and the SHCS data. The discrepancy between the adsorption rates obtained using SHCS and that obtained from monitoring the adsorption over time might be due to experimental design. The data obtained using SHCS is collected after steady-state equilibrium has already been reached. For the adsorption experiment, there is no protein present at time zero and when PnA is first introduced into the flowcell there is not only a "lag time" for the protein molecules to diffuse to the surface,[8] but also depletion of the bulk concentration as PnA binds to GM_1. Although the depletion of the bulk concentration is replenished every 5 minutes with a fresh protein solution, this might not be fast enough to exchange the depletion of protein molecules in the interfacial layer near the surface before the protein concentration of the interfacial layer has dropped below the bulk protein concentration.

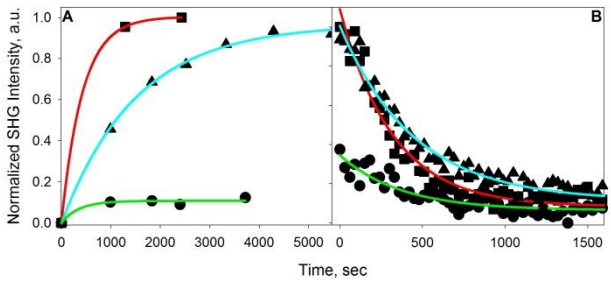

Figure S9. SH Intensity vs. time for (A) the adsorption and (B) desorption of PnA at a bulk protein concentration of 0.43 μM (●), 3 μM (▲), and 12 μM (■). Solid lines are fits to eq. S3 (A) and an exponential decay (B).

To validate this hypothesis, the SH intensity from the adsorption of PnA to GM_1 was monitored over time as a continuous flow of protein solution was flowed over the surface at a rate of 3 mL/min (data shown in Figure S10). Under continuous flow conditions there is a decrease in the time to reach a steady-state response as compared to when multiple injections are

made over time. The k_{on} for the continuous flow adsorption were calculated to be $1.4 \pm 0.4 \times 10^4$ $M^{-1}s^{-1}$, $1.1 \pm 0.1 \times 10^3$ $M^{-1}s^{-1}$, and $8.8 \pm 2.6 \times 10^2$ $M^{-1}s^{-1}$ for PnA concentrations 0.43 μM, 3 μM and 12 μM ,respectively. The fact that k_{on} increases by an order of magnitude when the fresh protein solution is continuously flowed over the surface as compared to adding fresh protein solution incrementally over time is evidence that mass transport is influencing the measured k_{on}, leading to a lower predicted adsorption rate than what actually exists. For the SHCS data, this mass transport effect on the binding kinetics is not present and as a result the calculated binding kinetics are drastically different from those calculated using binding isotherms where there are mass transport effects.

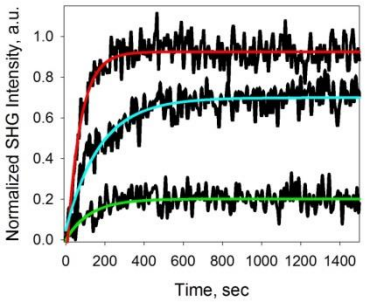

Figure S10. SH Intensity vs. time for the continuous flow adsorption of 0.43 μM (bottom), 3 μM (middle), and 12 μM (top) PnA bulk concentration. Solid lines are fits to eq. S3.

References

(1) Kriech, M. A.; Conboy, J. C. *J. Opt. Soc. Am. B: Optical Physics* **2004**, *21*, 1013.
(2) Shen, Y. R. *The Principles of Nonlinear Optics*; Wiley: New York, 1984.
(3) Nguyen, T. T.; Conboy, J. C. *Anal. Chem.* **2011**, *83*, 5979.
(4) Shi, J.; Yang, T.; Kataoka, S.; Zhang, Y.; Diaz, A. J.; Cremer, P. S. *JACS* **2007**, *129*, 5954.
(5) Janshoff, A.; Steinem, C.; Sieber, M.; Galla, H.-H. *Euro.Biophys. J.* **1996**, *25*, 105.
(6) Sanner, M. F. *Python: A Programming Language for Software Integration and Development*; J. Mol. Graphics Mod., 1999; Vol. 17.
(7) Nguyen, T. T.; Sly, K. L.; Conboy, J. C. *Anal. Chem.* **2012**, *84*, 201.
(8) Duverger, E.; Frison, N.; Roche, A.-C.; Monsigny, M. *Biochimie* **2003**, *85*, 167.